Apart from its basic function the plasma membrane Ca^{2+}ATPase regulates Ca^{2+} signaling by controlling phosphatidylinositol-4,5-bisphosphate levels

John T. Penniston[1,4,5], Rita Padányi[2,5], Katalin Pászty[3], Karolina Varga[1], Luca Hegedűs[1] and Agnes Enyedi[1,2] *

[1]Institute of Molecular Pharmacology, Research Centre for Natural Sciences, Hungarian Academy of Sciences, Budapest, Hungary

[2]Hungarian National Blood Transfusion Service, Budapest, Hungary

[3] Molecular Biophysics Research Group of the Hungarian Academy of Sciences and Department of Biophysics, Semmelweis University, Budapest, Hungary

[4]Department of Neurosurgery, Massachusetts General Hospital, Boston, Massachusetts 02114

[5]These authors contributed equally to this work.

*Corresponding author: Agnes Enyedi, Hungarian National Blood Transfusion Service, 1113 Budapest, Diószegi u. 64, Hungary. Tel/Fax: (361) 372-4353, e-mail:enyedi@biomembrane.hu

Running title: PMCAs control PIP_2 levels

Keywords: plasma membrane calcium ATPase (PMCA) / phosphatidylinositol-4,5,-bisphosphate (PIP_2) / Ca^{2+} signaling / molecular dynamics simulation.

JCS Advance Online Article. Posted on 6 November 2013

Summary

Plasma membrane Ca^{2+} ATPases (PMCAs) are known targets of phosphatidylinositol-4,5-bisphosphate (PIP_2), but if and how they control the PIP_2 pool has not been considered. We demonstrate here that PMCAs protect PIP_2 in the plasma membrane. Comparison of active and inactive PMCAs indicates that the protection operates by 2 mechanisms; one requiring active PMCA, the other not. It appears that the mechanism requiring activity is the removal of the Ca^{2+} required for sustained phospholipase C (PLC) activity, while the mechanism not requiring activity is PIP_2 binding. We show that in PMCA overexpressing cells, PIP_2 binding can lead to less IP_3 and diminished Ca^{2+} release from intracellular Ca^{2+} pools. Inspection of a homology model of PMCA suggests that PMCAs have a conserved cluster of basic residues forming a "blue collar" at the interface between the membrane core and the cytoplasmic domains. By molecular dynamics simulation we found that the blue collar forms four binding pockets for the phosphorylated inositol head group of PIP_2; these pockets bound PIP_2 strongly and frequently. Our studies suggest that by having the ability to bind PIP_2, PMCAs can control the accessibility of PIP_2 for PLC and other PIP_2 mediated processes.

Introduction

The plasma membrane Ca^{2+} ATPase (PMCA) belongs to the P-type ATPase family. Its major role is to remove excess Ca^{2+} from the cytosol and maintain intracellular Ca^{2+} homeostasis essential for the living cell (Brini and Carafoli, 2009; Strehler et al., 2007). The primary structure of PMCA shows about 30 % homology with that of the sarco/endoplasmic reticulum Ca^{2+} ATPase (SERCA) having highly conserved sequence motifs which are common to most P-type ATPases (Verma et al., 1988). Information about the tertiary structure is not available for the PMCAs because it is difficult to crystallize them; therefore, crystal structures of other members of P-type ATPases (Bublitz et al., 2010; Toyoshima et al., 2000) are used to make structural predictions (Bublitz et al., 2011). According to these predictions, the overall cytoplasmic domain arrangement of the PMCA is similar to that of SERCA except that PMCAs have two additional relatively large inserts; one connects the A domain with transmembrane helix 3 while the other is a long C-terminal tail having binding sites for Ca^{2+}-calmodulin and other regulatory elements.

There are 4 isoforms of PMCAs (PMCA1-4). Alternative splicing at splice sites "A" (variants x, y, z, w) and "C" (variants a, b, c) results in more than 20 PMCA variants (Strehler and Zacharias, 2001). According to their activation kinetics with Ca^{2+}-CaM the PMCAs are being classified as "slow" and "fast" pumps (Caride et al., 2001). It has long been known that besides of the activation with Ca^{2+}-CaM the activity of the PMCA is also increased by acidic phospholipids. Compared with other acidic lipids, however, lower concentrations of PIP_2 are required for their activation (Choquette et al., 1984; Lehotsky et al., 1992; Missiaen et al., 1989a; Missiaen et al., 1989b). Early proteolysis (Enyedi et al., 1987; Zvaritch et al., 1990) and peptide binding (Brodin et al., 1992; Filoteo et al., 1992) studies identified an acidic lipid binding sequence, the so-called AL region, close to transmembrane segment M3. This sequence has eight candidate residues that if exposed could provide positively charged side-chains for the electrostatic interaction with the lipids. Recent studies showed that deletions and/or mutations within/or close to this putative lipid-binding region activated the pump like acidic lipids did (Brini et al., 2010; Pinto and Adamo, 2002).

PIP_2 is a second messenger of the phospholipase C (PLC) signaling pathway (Berridge, 2009), and regulates a list of cellular functions including membrane targeting (Schill and Anderson, 2009), cytoskeletal reorganization (Moss, 2012), endocytosis and exocytosis (Koch and Holt, 2012), as well as, a variety of ion channels and receptors (Lemonnier et al., 2008; Michailidis et al., 2007; Michailidis et al., 2011; Suh and Hille, 2008; Trebak et al., 2009; Zhao et al., 2007). PIP_2 also interacts with many different proteins through either unstructured basic residue-rich regions or more-structured domains such as the pleckstrin homology (PH); Tubby; Fab1, YOTB, Vac1 and EEA1 (FYVE); Phox homology (PX); epsin N-terminal homology (ENTH); Clathrin Assembly Lymphoid Myeloid

(CALM); phosphotyrosine binding (PTB) and 4.1, ezrin, radixin, moiesin (FERM) domains, and regulates their activity and/or localization (Balla, 2005; McLaughlin and Murray, 2005; McLaughlin et al., 2002).

In the last two-three decades we have learned how the overall level of PIP_2 in the membrane is modulated by PIP kinases and phospholipase C. However, it has become evident that specific membrane microdomains of high PIP_2 levels are formed by complexes of proteins with PIP_2. Such proteins have been called PIPmodulins (Gamper and Shapiro, 2007; Lanier and Gertler, 2000). In the brain the more basic myristoylated alanine-rich C-kinase substrate (MARCKS) proteins have been implicated as major collectors of PIP_2 molecules (Kwiatkowska, 2010). Recent experiments suggested that syntaxin-1A could also induce PIP_2 segregation and PIP_2 could sequester syntaxin-1A into distinct lipid/protein clusters (van den Bogaart et al., 2011).

Here we show for the first time that PMCAs can serve as PIPmodulins because they attract PIP_2 molecules and protect them from excessive depletion by phospholipase C. We also show that PMCA expression decreases receptor-mediated inositol 1,4,5-triphosphate (IP_3) formation and hence, Ca^{2+} release from intracellular pools. Molecular dynamics simulation revealed a region of positively charged side-chains which appears to interact more strongly with PIP_2 than does the previously described AL region.

Results:

Experimental design to study the role of PMCA in PIP_2 signaling. Earlier a FRET-based direct binding assay suggested strong interaction between the purified erythrocyte PMCA pump and PIP_2 (Lehotsky et al., 1992). Here we wanted to see how PMCA affected PIP_2 signaling in live cells. In order to study this we used 3 species of PMCA and two types of HeLa cells in five distinct experimental setups: 1) sh-HeLa, in which the endogenous PMCA4 was knocked down to achieve the lowest possible PMCA level (Supplementary Figure S1); 2) sh-HeLa overexpressing PMCA2wb, the "w" splice variant of PMCA2b, which is a rapidly activated "fast" PMCA isoform produced by gene ATP2B2 (Caride et al., 2001); 3) wild type HeLa, with small amounts of endogenous PMCA4 and PMCA1; 4) wild type HeLa overexpressing PMCA4b-LA, which is a localization mutant of the slowly activated PMCA4b produced by gene ATP2B4. The designation LA indicates mutation of three leucine residues to alanines at the extreme C-terminus of PMCA4b at positions 1167-1169 (highlighted in red letters on a grey background in the sequence of Figure S4). This mutant had the same enzymatic characteristics as the wild type PMCA4b pump but showed enhanced plasma membrane localization (Antalffy et al., 2013); and 5) wild type HeLa overexpressing a non-functional (dead) PMCA4b-($D^{672}E$)-LA mutant (hereafter referred to as dPMCA4b-LA; the location of the $D^{672}E$ mutation is shown in Figure S4 as a white letter on purple). Since this mutant could not transport Ca^{2+} (Adamo et al., 1995) it helped to

separate the Ca^{2+} extrusion from the PIP_2 binding characteristics of the pump. This set of five covered the range from cells almost lacking PMCA (1 & 3) through cells containing an intact but inactive PMCA (5), cells containing large amounts of a "slow" PMCA (4), to cells containing large amounts of a "fast" PMCA (2). The relative levels of PMCA expression in the different cell types and the different experimental setups are shown in the Supplementary Figure S1. It is important to note that the expression levels of the different PMCA constructs are comparable, and about 100 times higher than that of the endogeneous pumps in wild type HeLa cells.

In our studies we also used four fluorescent reporter molecules. GFP or mCherry was covalently attached to PMCA and allowed visualization of the PMCA location. The third reporter molecule, $PH_{PLC\delta1}$-RFP (which has the pleckstrin homology (PH) domain of $PLC_{\delta1}$ fused to RFP) (Szentpetery et al., 2009; Varnai and Balla, 2008) is a sensor of PIP_2 and of IP_3 molecules. We will refer to this one as the PIP_2 sensor. The fourth reporter, GCaMP2, is a sensor of the intracellular Ca^{2+} concentration.

PMCAs protect PIP_2 molecules from ionomycin induced hydrolysis. Figure 1 shows how the intracellular distribution of the PIP_2 sensor was affected by expression of PMCA when Ca^{2+} was introduced into the cell. Before introduction of Ca^{2+} by addition of ionomycin, the PIP_2 sensor localized mainly in the plasma membrane either when expressed alone or together with PMCA2wb or PMCA4b-LA. The graphs show the PIP_2 sensor (red) and PMCA (green) signal intensity profiles along the line of interest marked on the confocal images.

Ionomycin treatment increases $[Ca^{2+}]_i$. which leads to the activation of PLC and then PIP_2 hydrolysis, resulting in the translocation of the PIP_2 sensor from the plasma membrane to the cytosol (Szentpetery et al., 2009). When the PIP_2 sensor moves from the plasma membrane to the cytosol, this reflects both the reduction of PIP_2 in the plasma membrane and the generation of IP_3 in the cytoplasm (Hirose et al., 1999). Figure 1B shows that PMCAs dramatically reduce movement of the PIP_2 sensor during ionomycin treatment. In the absence of PMCA, the PIP_2 sensor was distributed homogeneously over the entire cell while in cells expressing GFP-PMCA4b-LA or GFP-PMCA2wb high PIP_2 sensor signal was detected in the plasma membrane even after the ionomycin treatment (see the graphs in Figure 1).

To study further the effect of PMCAs on the distribution of PIP_2, cells were exposed to increasing concentrations of ionomycin (Figure 2). The pictures in Figure 2A show images of localization of the PIP_2 sensor before treatments and after 5 minutes of the addition of 2, 5 and 10 μM ionomycin, as indicated. The images of Figure 2A compare the effect of PMCA4b-LA (*bottom*) with control wild type HeLa cells (*middle*) and cells in which PMCA4 is suppressed (sh-HeLa cells; *images on the top*). The graphs of Figure 2B show time courses of the changes in the cytosolic fluorescence intensities of the PIP_2 sensor whereas the bar graph in Figure 2C shows the frequency of cells responding to a given

ionomycin concentration with complete translocation of the sensor. Experiments of this sort allowed us to classify cells according to their sensitivity to ionomycin. In Figure 2B the signal measured in sh-HeLa cells are shown in grey color. The light grey curve shows the averaged responses of highly ionomycin-sensitive cells (18% of total sh-HeLa cells) in which addition of 2 μM ionomycin induced full translocation of the PIP_2 sensor from the plasma membrane to the cytosol. 24% of cells (medium gray curve) responded to 5μM ionomycin and the remaining cells (dark gray curve in Figure 2B) responded to 10 μM ionomycin resulting in full PIP_2 sensor translocation in all sh-HeLa cells (see also Supplementary Movie S1). Expression of GFP-PMCA2wb in sh-HeLa cells protected the PIP_2 pool so that the sensor remained in the plasma membrane region during the ionomycin treatment even at high (10 μM) ionomycin concentration (red curve in Figure 2B). Similarly, ionomycin could not destroy PIP_2 and the PIP_2 sensor remained in the plasma membrane when GFP-PMCA4b-LA was expressed in wild-type HeLa cells (blue curve; Supplementary Movie S2).

To show the effect of an inactive PMCA in sequestering and protecting the PIP_2 molecules in the plasma membrane, we used the GFP-tagged inactive dPMCA4b-LA mutant. Figures 2B and 2C show that in HeLa cells expressing the inactive pump high (10 μM) ionomycin concentration was required to induce substantial movement of the PIP_2 sensor into the cytosol while lower ionomycin concentrations caused translocation of the PIP_2 sensor in only a few cells (Figure 2C). In contrast 27% of wild type HeLa cells expressing endogenously low amounts of PMCA4b and PMCA1b responded to 5 μM ionomycin. Unlike sh-HeLa, however, none of the wild type HeLa cells responded to 2 μM ionomycin indicating that the endogenous pumps may also provide some protection from PLC. Addition of 10 μM ionomycin, on the other hand, induced translocation of the sensor in all wild type or sh-HeLa cells. From these experiments it is evident that functional PMCAs can protect the PIP_2 pool from an excess Ca^{2+} overload and PLC activation. The comparison of the dPMCA4b-LA expressing cells with the wild type HeLa cells in Figure 2C suggests that even the inactive PMCA mutant could provide a significant shielding of PIP_2 from hydrolysis.

We also examined how the different PMCA variants affected the Ca^{2+} transients during the ionomycin treatments (Figure 3) by repeating the same experiments as above, using the GCaMP2 Ca^{2+} sensor to monitor $[Ca^{2+}]_i$ and mCherry-tagged PMCAs (see Figure S1). In sh-HeLa cells ionomycin induced long lasting Ca^{2+} increases and a high final signal value (Figure 3B black curve). In cells expressing mCherry-PMCA2wb addition of ionomycin induced only small and short-lived Ca^{2+} signals (*red curve*) explaining why the PIP_2 sensor was not translocated in the corresponding experiments. Expressing the mCherry-PMCA4b-LA pump the ionomycin-evoked Ca^{2+} signals (*blue curve*) were much larger than in the PMCA2wb expressing cells although they were somewhat less pronounced than in the sh-HeLa cells. In cells expressing the inactive dPMCA4b-LA the $[Ca^{2+}]_i$ response upon

ionomycin stimulation (*turquoise curve*) was greater than that measured in PMCA4b-LA expressing cells, as expected. The response of the dPMCA4b-LA expressing cells was similar to that of the wild type HeLa cells in this respect (not shown).

PMCAs reduce the receptor mediated PIP_2 signals. To study further the role of the PMCAs in PIP_2 signaling we induced activation of PLC through G protein-coupled receptors. In this case, initial activation of PLC does not need an increase in $[Ca^{2+}]_i$. Instead, PLC is activated through G-proteins to hydrolyze PIP_2 and release IP_3 which then stimulates Ca^{2+} release from the endoplasmic reticulum (ER) (Berridge, 2009). An example of the type of protocol used in our experiments is shown in the supplementary Figure S2. First the PLC signaling pathways were activated with a saturating concentration of extracellular ATP. After stimulation purinergic receptors quickly desensitize (Mundell and Kelly, 2011) therefore we used histamine, another G-protein coupled agonist, to test how effectively the cells can respond to a second stimulus. Both receptor stimuli were done in a calcium-free medium to show only the IP_3-mediated signal. It is clear from Figure S2 that in response to ATP stimulation only a fraction (10-20 %; see also Figure 4A1 and 4B1)) of total PIP_2 is degraded inducing robust Ca^{2+} release from the internal stores in good accordance with recent findings (Dickson et al., 2013). After 5 minutes calcium was added back to the medium to allow the entry of extracellular calcium into the cells via channels opened by the low concentration of Ca^{2+} in the lumen of the ER (Store-operated Ca^{2+} entry: SOCE) (Bird et al., 2008). Finally, we added a high concentration of ionomycin to evoke maximal response of the system.

Next, we examined how PMCAs affected IP_3 formation and the calcium signal in the absence of external Ca^{2+}. In both HeLa and sh-HeLa cells addition of ATP resulted in a sustained increase in the cytosolic intensity of the PIP_2 sensor indicating a substantial release of IP_3 (Figure 4A1 and 4B1, *black curves*). In good correlation with the elevated IP_3 concentration, the corresponding Ca^{2+} signaling experiments in Figure 4A2 and 4B2 (black curves) show a rapid Ca^{2+} release from the internal store followed by a slowly descending phase. The subsequent histamine stimulus resulted in only minor peaks of both IP_3 and Ca^{2+} superimposed on the first one suggesting that the freely available PIP_2 and/or ER resources were largely depleted. The shape of the Ca^{2+} signals was similar in both wild type HeLa and sh-HeLa cells (Figure 4A2 and 4B2) and the area under the ATP peaks was not significantly different between the two types of cells (Figure 4C1).

In contrast, in HeLa cells overexpressing PMCA4b-LA, ATP caused a much shorter Ca^{2+} peak followed by a short histamine-induced secondary response (Figure 4B2, *blue curve*). Consistent with this, the translocation of the PIP_2 sensor was also less pronounced (Figure 4B1) and the signal decayed after the ATP and histamine stimuli indicating quick relocation of the sensor to the plasma membrane in the PMCA4b-LA expressing cells. Strikingly, the Ca^{2+} signals in cells expressing PMCA4b-LA or

the inactive dPMCA4b-LA were almost identical during the early period of agonist stimulation in the absence of extracellular Ca^{2+} (Figures 4B2 and 4C1). The fact that Ca^{2+} returned to the baseline level in case of the inactive dPMCA4b-LA underlines the importance of other mechanisms (SERCA pump and/or the mitochondria) in eliminating Ca^{2+} from the cytosol. The signals of the PIP_2 sensor were also similar although, the cells with the inactive dPMCA4b-LA showed a slightly higher peak after the first stimulus than the cells with the active pump (Figure 4B1). These experiments suggested that during the early period of agonist stimulation the slow PMCA4 variant did not act through its Ca^{2+} removing ability but rather through its ability to bind PIP_2 making it less accessible for the PLC. To fulfill this role probably a relatively large amount of pump is required that is accomplished by the transient transfection in our experiments (Supplementary Figure S1B).

The PIP_2 sensor signal was similar in cells expressing either the "fast" PMCA2wb or the "slow" PMCA4b-LA pumps (Figures 4A1 and 4B1) suggesting that the PIP_2 binding capacity of both pumps was similar. The Ca^{2+} transients, however, returned to the baseline level more quickly in cells expressing the "fast" PMCA2wb (Supplementary Figure S3A) indicating that in the "slow" PMCA4b-LA expressing cells mostly the PIP_2 binding ability whereas in the case of the "fast" PMCA2wb expressing cells both the PIP_2 binding and pumping function contributed to the attenuation of the IP_3 mediated Ca^{2+} signal. Control experiments in Supplementary Figure S3B show that expression of the PIP_2 sensor alone had no effect on the Ca^{2+} signal suggesting that the sensor does not interfere with PIP_2 hydrolysis, as expected (Szentpetery et al., 2009; van der Wal et al., 2001).

Figure 4 also shows that the calcium pumping activity of PMCA4b-LA was essential in removing Ca^{2+} after Ca^{2+} entry through the plasma membrane Ca^{2+} channels. Adding Ca^{2+} back to the PMCA4b-LA expressing cells after ER store depletion resulted in a Ca^{2+} peak with smaller amplitude and shorter period than that observed in wild type HeLa cells. Here we found a pronounced difference between cells expressing the active or the inactive dPMCA4b-LA; in the dPMCA4b-LA expressing cells the Ca^{2+} curve had a long lasting decay phase similarly to the control cells (Figures 4B2 and C2). These results are in accordance with previous findings on the role of the PMCA in shaping Ca^{2+} entry mediated responses (Bautista et al., 2002; Bautista and Lewis, 2004; Ritchie et al., 2012; Snitsarev and Taylor, 1999).

Molecular dynamics simulation revealed four PIP_2 binding pockets around the neck of the PMCAs forming a "blue collar". Next we wanted to understand how PMCAs provide such a protecting environment for the PIP_2 molecules. The model of PMCA in the E1 conformation (see Methods) disclosed a collar of positively charged residues (Arg & Lys) at the cytoplasmic face of the membrane (Figure 5A). The next three images in Figure 5 are surface electrostatic potential representations of B, the same molecule; C, a hypothetical molecule missing the PMCA specific inserts (these include the

AL region and the complete C-tail); and D, the E1 conformation of SERCA (1T5S). These maps show a nearly continuous positive surface potential around the neck (the "blue collar") of the PMCA that must arise from a cluster of basic residues. The previously identified lipid-binding domain (AL) was a stretch of 25 amino acids which were contiguous in the primary sequence of PMCA. In contrast, the "blue collar" is composed of residues from all parts of the stalk regions of PMCA which is also present in the hypothetical PMCA molecule missing the AL region (Figure 5C). The blue collar residues are assembled into a coherent structure when the secondary and tertiary structures of PMCA are formed. The molecule in the right is SERCA which lacks nearly all basic residues in the stalk region (supplementary Figures S4 and S5) and therefore, the blue collar, as well.

In order to observe if and where the PIP_2 molecules bind to the blue collar, fifteen molecular dynamics runs were carried out; each run lasted 10 nsec and contained 5 PIP_2, for a total of 75 PIP_2 molecules. Of these 75 molecules, 20 bound to one residue, 24 bound to more than one amino acid residue and 31 remained unbound. A PIP_2 molecule was considered bound when it remained within 4.0 Å of a PMCA residue for many nsec. Each run showed a different pattern of binding because of the randomness of the original PIP_2 positions, but these runs disclosed 4 pockets of positively charged residues which bound PIP_2.

The images in Figure 6A and B show the four binding pockets; left to right, they are K173 (red), R993 (green), K980 (purple) and R914 (blue). Of the 24 multiply bound PIP_2s, 8 bound to pocket R993, 7 to R914, 5 to K980, 3 to K173 and 1 in an unusual way to residues K365 and K909. The interaction energies of the PIP_2s with their binding pockets are summarized in Figure 6D. Since it was only possible to do 10 nsec runs, it is probable that these PIP_2s are not yet in their most favorable positions relative to the binding pocket. This point of view is reinforced by the observation that the positions of PIP_2s in the different runs are different. For comparison, the interaction energy was calculated for a PIP_2 binding site from a K-channel (3SPI) (Hansen et al., 2011). Since this structure was that of a crystal, we would expect the PIP_2 and the binding pocket to be closer to their most favorable position. This is probably why the interaction energy is stronger for 3SPI than the strongest interaction in PMCA.

The strongest interaction energy for a binding of PIP_2 to R993 was -609 kcal/mol, about 62% of the -977 kcal/mol found for binding of PIP_2 to its site in the K-channel (Hansen et al., 2011). The strength of the interaction of PIP_2 with R993 shows that its binding is probably biologically significant.

Table 1 shows that PIP_2 binds to amino acid residues more strongly than other phospholipids do. PIP_2 also binds more frequently to multiple residues. Not only does PIP_2 have a higher negative charge than the other lipids, but its negative charge is in two locations, the P1 phosphorus atom and the P4 & P5

phosphorus atoms. The P1 atom is closer to the surface of the membrane, where it can bind to the lower part of the blue collar, while the P4 and P5 atoms are further from the membrane surface and can bind to the upper parts of the blue collar.

This charge distribution of PIP_2 contributes especially strongly to its binding to pocket R993. The alignments of Supplementary Figures S4 and S5 show the alpha carbon of residue R993 in the middle of transmembrane helix M9. In the 3D model, residue R993 reaches toward the cytoplasm, so that the charged guanido group is in the amphiphilic boundary layer between the membrane's hydrophobic core and the cytoplasm. Here it is positioned so that it will interact with the P1 charged group of PIP_2 and other anionic lipids, as shown in Figure 6C.

Discussion

All of the studies reported here were done with overexpressed PMCA and with models. Nonetheless, they have provided useful information about the binding of PIP_2 to PMCA which suggests new roles for PMCA in managing the Ca^{2+} signal. It has long been known that PMCA pumps Ca^{2+} out of cells and that PIP_2 stimulated that activity. By using a PIP_2 sensor we found that expression of PMCA protects PIP_2 molecules from hydrolysis by PLC and that the protection operates by two mechanisms. One requires only an intact PMCA (no activity is required), the second requires a fully active PMCA. The presence of a buffering mechanism by which inactive PMCA acts suggests that PMCAs must bind PIP_2 and create a PIP_2 pool which is probably in equilibrium with free PIP_2 molecules in the plasma membrane. Hence, the retention of the PIP_2 sensor in the plasma membrane upon expression of the inactive PMCA is due to the binding of the sensor to the free PIP_2 molecules, which are maintained in equilibrium with the PIP_2 bound by the PMCA. The role of such a PIP_2 buffering mechanism has been described recently showing that the MARCKS protein can regulate the activity of TRPC1 channel via buffering PIP_2 molecules in the vicinity of the channel (Shi et al., 2013).

In general, cells express small amounts of PMCAs; red blood cells for example express only 35 copies per square micron which is much less than the abundance of the PIP_2 molecules (about 5000 - 10000 per square micron; (Suh and Hille, 2008)) in the plasma membrane. We suggest that buffering PIP_2 by the PMCAs might have a substantial impact on PIP_2 signaling when a large amount of pump is being expressed at discrete locations like the dendritic spines or the stereocilia of hair cells (Burette et al., 2010; Zhao et al., 2012). We must emphasize, however, that even a small amount of active PMCA could be protective if located near the PIP_2 pool. The PMCA-PIP_2 pool could have a great importance in PIP_2 related processes by i) preventing complete depletion of PIP_2 and ii) encouraging the formation of extensive PIP_2-rich areas in specific membrane locales where PMCA is abundant.

Calculation of the electrostatic potential at the surface of a PMCA4b model disclosed a positively charged electrostatic patch around the stalk region of the molecule that we called the blue collar. Molecular dynamics simulation experiments revealed four PIP_2 binding pockets formed from the blue collar residues of PMCA4b. Based on these findings we propose that PIP_2 interacts not only through non-specific electrostatic interactions with the previously described (Brodin et al., 1992; Filoteo et al., 1992) lipid-binding AL sequence but also through specific interactions by fitting its phosphatidylinositol head-group into binding pockets. Specific pocket binding of the PIP_2 head is also used by other molecules. X-ray crystal structures of the Kir2.2 (Hansen et al., 2011) and GIRK2 K^+ (Whorton and MacKinnon, 2011) channels have identified highly specific phosphatidylinositol-binding regions at an interface between the transmembrane domain and the cytoplasmic domains of these molecules. Also, several phosphoinositide-binding signal molecules use structured domains to achieve specific recognition of different phosphoinositide headgroups (Kutateladze, 2010).

Figures S4, S5 and S6 show the relationship of the human hPMCA4b to other PMCAs and SERCA. Figure S5 shows that the four genes which code for human PMCA retain almost all of the residues which make up the blue collar. Of the residues which compose the binding sites (highlighted in cyan), the only exceptions are R993 (missing in hPMCA3 and hPMCA1), R1052 (present only in hPMCA4) and K89 (missing in hPMCA3). This figure also shows that SERCA1a does not retain any corresponding residues, except for R438, R439 and K442. In many of the corresponding positions, SERCA1a has acidic residues instead of basic ones. These relationships indicate that the PIP_2 binding sites of PMCA have special functions not shared by SERCA.

Figure S6 shows that the PIP_2 binding sites are conserved in PMCAs throughout the animal kingdom. From humans to fish and insects the binding residues are almost always retained. However, in other organisms (plants and prokaryotes) PMCA-type molecules have very different structures not only in the blue collar region, but also in most other parts of the molecule. Figure S4 shows the alignment of the whole SERCA and PMCA sequences which were used for constructing the model.

The properties of PMCA reported here suggest that it may function as a unique PIPmodulin that mediates PIP_2 clustering at specific locations. Since PMCA binds PIP_2 and provides a low Ca^{2+} milieu; it may form a *Ca^{2+}-less PMCA-PIP_2-Pool* (CPPP) in the cell membrane. The known PIPmodulins such as the myristoylated alanine-rich C-kinase substrate (MARCKS), growth-associated protein-43 (GAP43) and cytoskeleton-associated protein (CAP23) also sequester PIP_2 molecules (Laux et al., 2000), but when they bind Ca^{2+}-calmodulin these PIPmodulins release PIP_2. In contrast, as is seen in Figures 1 & 2, PMCA keeps PIP_2 in the plasma membrane even in the presence of elevated Ca^{2+}. PIP_2 also enhances the activity of the PMCAs; this would be expected to reduce the Ca^{2+} concentration in

the vicinity of the CPPP, reducing the activity of PLC and stabilizing the PMCA bound PIP_2 compartment.

Moreover, there are certain plasma membrane compartments with high PIP_2 content where the members of the MARCKS family are not expressed and the putative PIPmodulin is likely to be PMCA. 3D simulations suggest that local sequestration of PIP_2 in the spine heads of Purkinje neurons is responsible for the observed IP_3 signalling (Brown et al., 2008). MARCKS, GAP43 or CAP23 are not found in Purkinje cells (ConsoleBram et al., 1996; Ouimet et al., 1990) but PMCA2 is concentrated in the spine heads of Purkinje neurons (Burette et al., 2010). Another example where both PIP_2 and PMCA are abundant in the same specific compartment is the stereocilia of hair cells in the inner ear. In these regions of the hair cells about 2000 PMCA2 molecules are gathered in a square micron (Yamoah et al., 1998). If we take the assumption that about 5000 - 10000 PIP_2 molecules are in a square micron of the plasma membrane we may assume that most of them are sequestered by the large amount of PMCA in the stereocilia. In good accordance with this hypothesis, recent studies (Zhao et al., 2012) demonstrated that PIP_2 was concentrated at the tips of stereocilia together with the PMCA2 protein. Further experiments demonstrated that a specific asymmetric distribution of PIP_2 (Hirono et al., 2004) and PMCA2 (Kozel et al., 1998) was essential for the appropriate function of hair cells underlining the importance of a putative CPPP in hearing.

In summary, we suggest that by protecting PIP_2 molecules PMCA can mediate the cellular concentrations of two messenger molecules, IP_3 and Ca^{2+}, and hence may play a substantial role in the complex interplay between local PIP_2 and Ca^{2+} signaling. In addition, by PIP_2 binding PMCAs can affect many cellular functions regulated by PIP_2 such as the activity of channels and pumps, remodelling of the actin cytoskeleton, endocytosis and migration. Finally, imbalances of the PIP_2/PIP_3 phospholipids may cause defects in cell functions leading to cancer and other diseases. Therefore, controlling the level of these molecules by PMCAs may protect cells against such diseases.

Materials and methods:

Reagents and antibodies. Fugene HD Transfection Reagent was obtained from Roche Applied Science (Mannheim, Germany). All other chemicals used were of reagent grade.

DNA constructs. The mammalian expression construct for $PH_{PLC\delta1}$-RFP was a kind gift from Péter Várnai (Semmelweis University, Hungary) and was described previously (Varnai and Balla, 2008). pN1-GCaMP2 plasmid was a kind gift of Junichi Nakai, RIKEN Brain Science Institute, Saitama, Japan (Nakai and Ohkura, 2003).Generation of the pEGFP-PMCA2wb plasmid was described previously (Chicka and Strehler, 2003). The mCherry-PMCA2wb construct was created by replacing

the EGFP fragment of pEGFP-PMCA2wb plasmid with the mCherry coding sequence from the pmCherry-C1 vector (Clontech) using the *Age*I-*Kpn*I restriction sites. The pEGFP-PMCA4b-$L^{1167\text{-}69}A$ (hereafter called GFP-PMCA4b-LA) plasmid was constructed as described (Antalffy et al., 2013). To create mCherry-PMCA4b-$L^{1167\text{-}1169}A$ (hereafter called mCherry-PMCA4b-LA) construct, site directed mutagenesis introducing the $L^{1167\text{-}1169}A$ triple mutation was performed on the mCherry-PMCA4b template plasmid (Antalffy et al., 2013) using the QuikChange II Site-Directed Mutagenesis Kit (Stratagene) with the following primers: forward 5'-CTAAGTTTGGGACTAGGGTGGCAGCGGCGGATGGTGAGGTCACTCCATATGCC-3', reverse 5'-GGCATATGGAGTGACCTCACCATCCGCCGCTGCCACCCTAGTCCCAAACTTAG-3'. pEGFP-PMCA4b-$D^{672}E$-$L^{1167\text{-}1169}A$ and mCherry-PMCA4b-$D^{672}E$-$L^{1167\text{-}1169}A$ constructs, hereafter called GFP-dPMCA4b-LA and mCherry-dPMCA4b-LA, were created by introducing the $D^{672}E$ point mutation to the PMCA4b-LA plasmids using the QuikChange II Site-Directed Mutagenesis Kit (Stratagene). PCR primers were as follows: forward 5'-GGTGGGCATTGAGGAGCCTGTGCGCCCAGAG-3', reverse 5'-CTCTGGGCGCACAGGCTCCTCAATGCCCACC-3'.

sh-HeLa cell line: sh-HeLa cell line was generated by using PMCA4 shRNA plasmid (Santa Cruz Biotechnology, Inc. sc-42602-SH). HeLa cells were transfected with PMCA4 shRNA plasmid or with control shRNA plasmid-A (sc-108060) in a six-well plate by using shRNA Plasmid Transfection Medium (sc-108062) and shRNA Plasmid Transfection Reagent according to the manufacture's protocol. 48hrs after transfection cells were selected by Puromycin dihydrochloride (2 µg/ml) (sc-108071) in DMEM for two weeks and medium was changed to fresh medium with Puromycin in every 2-3 days. After selection cell clones were prepared using cloning rings. PMCA4b expression was tested by Western Blot Analysis. From the most efficient clone sh-HeLa cell line was generated.

Cell Culture and Transfection. HeLa (obtained from ECACC) or sh-HeLa cells were grown in DMEM supplemented with 10% FBS, 100 U/ml penicillin, 100 µg/ml streptomycin and 2 mM glutamine under 5% CO_2 at 37 ^{o}C. One day prior to transfection cells were seeded into a Lab-Tek^{TM} II Chambered Slide (Nalge Nunc Int.) at 4-6 x 10^4 cell density. Transfection using the appropriate combination of plasmids described in Supplementary Figure S1 was carried out with FuGene HD (Roche) according to the protocol of the manufacturer. This procedure yielded about 60-70 % transfected cells in the cell culture. Cells were inspected 24 hours after transfection.

Analysis of PIP_2 translocation and Ca^{2+} signaling by confocal imaging. HeLa or sh-HeLa cells were seeded into a Lab-Tek^{TM} II Chambered Slide (Nalge Nunc Int.) and transfected with $PH_{PLC\delta1}$-RFP alone or together with GFP-tagged PMCA constructs for the PIP_2 translocation experiments; or with GCaMP2 alone or together with mCherry-tagged PMCA constructs for Ca^{2+} imaging (Supplementary

Figure S1). Prior to the measurement of sensitivity of cells to ionomycin the culture media was replaced with Hank's Buffered Salt Solution (HBSS) supplemented with 0.9 mM $MgCl_2$, 2 mM $CaCl_2$ and 20 mM Hepes (pH 7.4). Cells were sequentially exposed to 2 μM, 5 μM and 10 μM ionomycin at 0, 6 and 12 minutes. In order to study activation of the PLC pathway by G-receptor-coupled agonists the culture media was replaced with nominally Ca^{2+} free HBSS supplemented with 0.9 mM $MgCl_2$, 100 μM EGTA, 100 μM $CaCl_2$ and 20 mM Hepes (pH 7.4)). Cells were stimulated by the consecutive additions of 100 μM ATP and 100 μM histamine (at 0 and 2 minutes) in the absence of Ca^{2+} (*IP_3 mediated signal*). After 5 minutes incubation the extracellular medium was replenished by 2 mM Ca^{2+} and store operated Ca^{2+} entry (*SOCE signal*) was monitored for 5 more minutes. Finally, maximal response was induced by the addition of 10 μM ionomycin.

Images were taken with an Olympus IX-81 laser scanning confocal microscope and Fluoview FV500 software using an Olympus PLAPO 60× (1.4) oil immersion objective. For $PH_{PLC\delta1}$-RFP imaging cells were excited at 543 nm and emission was collected above 560 nm. For GCaMP2 imaging cells were excited at 488 nm and emission was collected between 505-535 nm. Region of interest was selected in the cytosol, nuclei were omitted. GFP-tagged PMCAs were illuminated at 488 nm and emission between 505-535 nm was recorded. mCherry-tagged PMCAs were illuminated at 543 nm and emission above 560 nm was recorded. Images were acquired every 0.3 – 1.2 s, z-resolution was 0.5 μm. Time lapse sequences were recorded with Fluoview Tiempo (v4.3) time course software at room temperature. The relative fluorescence was calculated as F/F_0 (where F_0 was the average initial fluorescence). GraphPad Prism4 software was used to analyze the experimental data.

Data analysis and statistics. Data presented in Figure 4 are means of at least three independent experiments ± S.E. and statistical significance was determined by Student's t-test. For statistical analysis of data in Figure 2, cells were scored according to the ionomycin concentration at which full translocation of the PIP_2 sensor occurred. Statistical significance of image scores was determined by the $\chi 2$ test.. Statistical analyses were performed using Excel software (Microsoft) and GraphPad Prism 4 software (GraphPad Software Inc.)

Construction of a model of PMCA4b. The calcium pump of rabbit sarcoplasmic reticulum SERCA1a has been crystallized at several stages of its catalytic cycle (Toyoshima et al., 2004; Toyoshima et al., 2009) and has considerable resemblance to PMCA4b. Figure S4 shows an alignment of these two pumps. Study of this figure shows that PMCA is longer than SERCA, the extra protein in PMCA being at the N- and C-terminal domains and in a long insert marked as I. Not including these 3 regions, the PMCA sequence contained 31% residues identical to SERCA, as well numerous similar

residues. In addition to sequence identities, proper positioning of the hydrophobic transmembrane regions assures an accurate alignment (PMCA and SERCA have 10 transmembrane regions each). The structures of the SERCA AMPPCP-Ca2 (1T5S & 1VFP) and of the N-domains of the Na,K ATPase (1MO7 & 1MO8) were aligned with PMCA4b and a model of PMCAE1 made. The alignment of PMCA4b with SERCA1a was the same as is shown in Figure S4. Modeller 8v2 was then used to create the PMCA model covering residues 1-1058. It has been reported that F1094 crosslinks to the peptide C537-ALLGFVT in the N domain (Carafoli et al., 1992; Falchetto et al., 1991; Falchetto et al., 1992). Accordingly, residues 1059-1094 (part of the C-terminus) were added next, with F1094 placed near C537. This caused the C-terminus to go away from the membrane interface, up over the cytoplasmic top of PMCA. The remainder of the C-terminus (residues 1095-1205) was modeled using Tasser (Roy et al., 2010) and attached to the end of PMCA.

In general, the subsequent work was done using CHARMM (Brooks et al., 1983); http://www.charmm.org/) and CHARMM-GUI (Jo et al., 2008); http://www.charmm-gui.org/). The PMCA was put into a hexagonal box with a lipid bilayer, TIP3 water and enough potassium ions and chloride ions to make a neutral system with 0.15 M salt. The lipid composition was chosen to approximate that of the plasma membrane of 3T3 fibroblasts (Pankov et al., 2006). The outer leaflet of the membrane contained 17 cholesterol molecules (CHL-13%), 82 of palmitoyloleylphosphatidylcholine (POPC-63%) and 31 of stearoylarachidonylphosphatidylcholine (SAPC-24%-representing sphingomyelin). The inner (cytoplasmic) leaflet contained 17 cholesterol molecules (CHL-13%), 31 of palmitoyloleylphosphatidylcholine (POPC-24%), 4 of palmitoyloleylphoshatidic acid (PA-3%), 42 of palmitoyloleylphosphatidylethanolamine (POPE-32%), 16 of palmitoyloleylphosphatidylserine (POPS-13%) 15 of stearoylarachidonylphosphatidylinositol (PI-12%) and 5 of stearoylarachidonylphosphatidylinositolbisphosphate (PIP_2-3%).

After minimization and heating, the molecular dynamics studies were done on this hexagonal box containing the 1205 residues of PMCA, 250 molecules of membrane lipid, 32074 TIP3 water molecules, 132 K^+ ions and 63 Cl^- ions at 310˚ K. The box was 104 Å on each side and its initial length was 155 Å. The early stages of the dynamics run were done at constant pressure and temperature; the dimensions of the box were allowed to vary to keep the pressure constant. After the initial fluctuations in the dimensions had diminished, the dimensions of the box were fixed and the run carried on at constant volume and temperature.

The electrostatic and van der Waals interaction energies between various atoms were calculated by CHARMM. These energies are calculated directly from the physical formulas, and so are the total energies rather than the energies with respect to a standard reference state. They also lack a PV term, but this does not affect the validity of the results, since the electrostatic energy is clearly the dominant term, and the one which changes the most.

In order to keep the molecular dynamics run times to reasonable values, a large portion of the atoms in the model were fixed in space. After the initial phase was running smoothly, all atoms in the

cytoplasmic half of the prism were fixed, as well as the backbone of the protein, the sidechains and waters in the extracellular part of the prism. This left the sidechains of the collar, the lipids of the membrane and nearby waters free to move.

Also because of time limitations, it was necessary to place the PIP_2 molecules near PMCA in order to observe the interactions within the 10 nsec of simulation. The 5 PIP_2 molecules were placed at random starting positions near the PMCA in order to sample all the possible binding sites. 15 runs of 10 nsec each were done, and the interactions of lipid with the protein observed in each.

Some variations from these conditions occurred. In the first two runs, the PIP_2 was not placed near PMCA, and only one interaction was observed. In some of the early runs, the side chains of the blue collar were not allowed to move.

Acknowledgements

We are grateful to Krisztina Lór for excellent technical assistance. Thanks to Junichi Nakai (RIKEN Brain Science Institute, Saitama, Japan) for providing the pN1-GCaMP2 plasmid, to Péter Várnai (Semmelweis University, Hungary) for the $PH_{PLC\delta1}$-RFP plasmid and to Robert Katona (Institute of Genetics, Biological Research Center of the Hungarian Academy of Sciences) for the pcDNA3-mCherry plasmid. The SB-CAG-Amaxa GFP vector was a gift of Tamás Orbán (Institute of Molecular Pharmacology, Research Centre for Natural Sciences, Hungarian Academy of Sciences).

This work was supported by grants from OTKA CK 80283 and K 101064 (AE) and TRANSRAT KMR_12-1-2012-0112 (KP).

Author contributions

JTP, RP and AE conceived the project and wrote the manuscript; RP and AE designed and performed the experiments, and analyzed the data; KP did the Ca^{2+} signaling experiments and analyzed the data; JTP developed the model and ran the molecular dynamics simulations; LH and KV designed, generated and validated the plasmid constructs; AE supervised and coordinated the project.

Conflict of interest

The authors declare that they have no conflict of interest.

References

Adamo, H. P., Filoteo, A. G., Enyedi, A. and Penniston, J. T. (1995). Mutants in the putative nucleotide-binding region of the plasma-membrane Ca^{2+}-pump - a reduction in activity due to slow dephosphorylation. *Journal of Biological Chemistry* **270**, 30111-30114.

Antalffy, G., Paszty, K., Varga, K., Hegedus, L., Enyedi, A. and Padanyi, R. (2013). A C-terminal di-leucine motif controls plasma membrane expression of PMCA4b. *Biochimica et Biophysica Acta-Molecular Cell Research* **1833**, 2561-2572.

Balla, T. (2005). Inositol-lipid binding motifs: signal integrators through protein-lipid and protein-protein interactions. *Journal of Cell Science* **118**, 2093-2104.

Bautista, D. M., Hoth, M. and Lewis, R. S. (2002). Enhancement of calcium signalling dynamics and stability by delayed modulation of the plasma-membrane calcium-ATPase in human T cells. *Journal of Physiology-London* **541**, 877-894.

Bautista, D. M. and Lewis, R. S. (2004). Modulation of plasma membrane calcium-ATPase activity by local calcium microdomains near CRAC channels in human T cells. *Journal of Physiology-London* **556**, 805-817.

Berridge, M. J. (2009). Inositol trisphosphate and calcium signalling mechanisms. *Biochimica et Biophysica Acta* **1793**, 933-40.

Bird, G. S., DeHaven, W. I., Smyth, J. T. and Putney, J. W. (2008). Methods for studying store-operated calcium entry. *Methods* **46**, 204-212.

Brini, M. and Carafoli, E. (2009). Calcium Pumps in Health and Disease. *Physiological Reviews* **89**, 1341-1378.

Brini, M., Di Leva, F., Ortega, C. K., Domi, T., Ottolini, D., Leonardi, E., Tosatto, S. C. E. and Carafoli, E. (2010). Deletions and Mutations in the Acidic Lipid-binding Region of the Plasma Membrane Ca^{2+} Pump A study on different splicing variants of isoform 2. *Journal of Biological Chemistry* **285**, 30779-30791.

Brodin, P., Falchetto, R., Vorheer, T. and Carafoli, E. (1992). Identification of 2 Domains Which Mediate the Binding of Activating Phospholipids to the Plasma-Membrane Ca2+ Pump. *European Journal of Biochemistry* **204**, 939-946.

Brooks, B. R., Bruccoleri, R. E., Olafson, B. D., States, D. J., Swaminathan, S. and Karplus, M. (1983). Charmm - a Program for Macromolecular Energy, Minimization, and Dynamics Calculations. *Journal of Computational Chemistry* **4**, 187-217.

Brown, S. A., Morgan, F., Watras, J. and Loew, L. M. (2008). Analysis of phosphatidylinositol-4,5-bisphosphate signaling in cerebellar Purkinje spines. *Biophysical Journal* **95**, 1795-1812.

Bublitz, M., Morth, J. P. and Nissen, P. (2011). P-type ATPases at a glance. *Journal of Cell Science* **124**, 2515-2519.

Bublitz, M., Poulsen, H., Morth, J. P. and Nissen, P. (2010). In and out of the cation pumps: P-Type ATPase structure revisited. *Current Opinion in Structural Biology* **20**, 431-439.

Burette, A. C., Strehler, E. E. and Weinberg, R. J. (2010). A plasma membrane Ca^{2+} ATPase isoform at the postsynaptic density. *Neuroscience* **169**, 987-993.

Carafoli, E., Kessler, F., Falchetto, R., Heim, R., Quadroni, M., Krebs, J., Strehler, E. E. and Vorherr, T. (1992). The Molecular-Basis of the Modulation of the Plasma-Membrane Calcium-Pump by Calmodulin. *Ion-Motive Atpases : Structure, Function, and Regulation* **671**, 58-69.

Caride, A. J., Filoteo, A. G., Penheiter, A. R., Paszty, K., Enyedi, A. and Penniston, J. T. (2001). Delayed activation of the plasma membrane calcium pump by a sudden increase in Ca2+: fast pumps reside in fast cells. *Cell Calcium* **30**, 49-57.

Chicka, M. C. and Strehler, E. E. (2003). Alternative splicing of the first intracellular loop of plasma membrane Ca^{2+}-ATPase isoform 2 alters its membrane targeting. *Journal of Biological Chemistry* **278**, 18464-18470.

Choquette, D., Hakim, G., Filoteo, A. G., Plishker, G. A., Bostwick, J. R. and Penniston, J. T. (1984). Regulation of Plasma-Membrane Ca-2+ Atpases by Lipids of the Phosphatidylinositol Cycle. *Biochemical and Biophysical Research Communications* **125**, 908-915.

ConsoleBram, L. M., FitzpatrickMcElligott, S. G. and McElligott, J. G. (1996). Distribution of GAP-43 mRNA in the immature and adult cerebellum: A role for GAP-43 in cerebellar development and neuroplasticity. *Developmental Brain Research* **95**, 97-106.

Dickson, E. J., Falkenburger, B. H. and Hille, B. (2013). Quantitative properties and receptor reserve of the IP3 and calcium branch of G(q)-coupled receptor signaling. *Journal of General Physiology* **141**, 521-535.

Enyedi, A., Flura, M., Sarkadi, B., Gardos, G. and Carafoli, E. (1987). The Maximal Velocity and the Calcium Affinity of the Red-Cell Calcium-Pump May Be Regulated Independently. *Journal of Biological Chemistry* **262**, 6425-6430.

Falchetto, R., Vorherr, T., Brunner, J. and Carafoli, E. (1991). The Plasma-Membrane Ca2+ Pump Contains a Site That Interacts with Its Calmodulin-Binding Domain. *Journal of Biological Chemistry* **266**, 2930-2936.

Falchetto, R., Vorherr, T. and Carafoli, E. (1992). The Calmodulin-Binding Site of the Plasma-Membrane Ca-2+ Pump Interacts with the Transduction Domain of the Enzyme. *Protein Science* **1**, 1613-1621.

Filoteo, A. G., Enyedi, A. and Penniston, J. T. (1992). The Lipid-Binding Peptide from the Plasma-Membrane Ca^{2+} Pump Binds Calmodulin, and the Primary Calmodulin-Binding Domain Interacts with Lipid. *Journal of Biological Chemistry* **267**, 11800-11805.

Gamper, N. and Shapiro, M. S. (2007). Target-specific PIP(2) signalling: how might it work? *Journal of Physiology-London* **582**, 967-975.

Hansen, S. B., Tao, X. and MacKinnon, R. (2011). Structural basis of PIP2 activation of the classical inward rectifier K+ channel Kir2.2. *Nature* **477**, 495-U152.

Hirono, M., Denis, C. S., Richardson, G. P. and Gillespie, P. G. (2004). Hair cells require phosphatidylinositol 4,5-bisphosphate for mechanical transduction and adaptation. *Neuron* **44**, 309-320.

Hirose, K., Kadowaki, S., Tanabe, M., Takeshima, H. and Iino, M. (1999). Spatiotemporal dynamics of inositol 1,4,5-trisphosphate that underlies complex Ca2+ mobilization patterns. *Science* **284**, 1527-1530.

Jo, S., Kim, T., Iyer, V. G. and Im, W. (2008). Software news and updates - CHARNIM-GUI: A web-based grraphical user interface for CHARMM. *Journal of Computational Chemistry* **29**, 1859-1865.

Koch, M. and Holt, M. (2012). Coupling exo- and endocytosis: An essential role for PIP2 at the synapse. *Biochimica Et Biophysica Acta-Molecular and Cell Biology of Lipids* **1821**, 1114-1132.

Kozel, P. J., Friedman, R. A., Erway, L. C., Yamoah, E. N., Liu, L. H., Riddle, T., Duffy, J. J., Doetschman, T., Miller, M. L., Cardell, E. L. et al. (1998). Balance and hearing deficits in mice with a null mutation in the gene encoding plasma membrane Ca^{2+}-ATPase isoform 2. *Journal of Biological Chemistry* **273**, 18693-18696.

Kutateladze, T. G. (2010). Translation of the phosphoinositide code by PI effectors. *Nature Chemical Biology* **6**, 507-513.

Kwiatkowska, K. (2010). One lipid, multiple functions: how various pools of PI(4,5)P-2 are created in the plasma membrane. *Cellular and Molecular Life Sciences* **67**, 3927-3946.

Lanier, L. M. and Gertler, F. B. (2000). Actin cytoskeleton: Thinking globally, actin' locally. *Current Biology* **10**, R655-R657.

Laux, T., Fukami, K., Thelen, M., Golub, T., Frey, D. and Caroni, P. (2000). GAP43, MARCKS, and CAP23 modulate PI(4,5)P-2 at plasmalemmal rafts, and regulate cell cortex actin dynamics through a common mechanism. *Journal of Cell Biology* **149**, 1455-1471.

Lehotsky, J., Raeymaekers, L., Missiaen, L., Wuytack, F., Desmedt, H. and Casteels, R. (1992). Stimulation of the Catalytic Cycle of the Ca2+ Pump of Porcine Plasma-Membranes by Negatively Charged Phospholipids. *Biochimica et Biophysica Acta* **1105**, 118-124.

Lemonnier, L., Trebak, M. and Putney, J. W. (2008). Complex regulation of the TRPC3, 6 and 7 channel subfamily by diacylglycerol and phosphatidylinositol-4,5-bisphosphate. *Cell Calcium* **43**, 506-514.

McLaughlin, S. and Murray, D. (2005). Plasma membrane phosphoinositide organization by protein electrostatics. *Nature* **438**, 605-611.

McLaughlin, S., Wang, J. Y., Gambhir, A. and Murray, D. (2002). PIP2 and proteins: Interactions, organization, and information flow. *Annual Review of Biophysics and Biomolecular Structure* **31**, 151-175.

Michailidis, I. E., Helton, T. D., Petrou, V. I., Mirshahi, T., Ehlers, M. D. and Logothetis, D. E. (2007). Phosphatidylinositol-4,5-bisphosphate regulates NMDA receptor activity through alpha-actinin. *Journal of Neuroscience* **27**, 5523-5532.

Michailidis, I. E., Rusinova, R., Georgakopoulos, A., Chen, Y. B., Iyengar, R., Robakis, N. K., Logothetis, D. E. and Baki, L. (2011). Phosphatidylinositol-4,5-bisphosphate regulates epidermal growth factor receptor activation. *Pflugers Archiv-European Journal of Physiology* **461**, 387-397.

Missiaen, L., Raeymaekers, L., Wuytack, F., Vrolix, M., Desmedt, H. and Casteels, R. (1989a). Phospholipid Protein Interactions of the Plasma-Membrane Ca-2+-Transporting ATPase - Evidence for a Tissue-Dependent Functional Difference. *Biochemical Journal* **263**, 687-694.

Missiaen, L., Wuytack, F., Raeymaekers, L., Desmedt, H. and Casteels, R. (1989b). Polyamines and Neomycin Inhibit the Purified Plasma-Membrane Ca-2+ Pump by Interacting with Associated Polyphosphoinositides. *Biochemical Journal* **261**, 1055-1058.

Moss, S. E. (2012). How Actin Gets the PIP. *Science Signaling* **5**.

Mundell, S. and Kelly, E. (2011). Adenosine receptor desensitization and trafficking. *Biochimica Et Biophysica Acta-Biomembranes* **1808**, 1319-1328.

Nakai, J. and Ohkura, M. (2003). Probing calcium ions with biosensors. *Biotechnology & Genetic Engineering Reviews, Vol 20* **20**, 3-21.

Ouimet, C. C., Wang, J. K. T., Walaas, S. I., Albert, K. A. and Greengard, P. (1990). Localization of the Marcks (87-Kda) Protein, a Major Specific Substrate for Protein Kinase-C, in Rat-Brain. *Journal of Neuroscience* **10**, 1683-1698.

Pankov, R., Markovska, T., Antonov, P., Ivanova, L. and Momchilova, A. (2006). The plasma membrane lipid composition affects fusion between cells and model membranes. *Chemico-Biological Interactions* **164**, 167-173.

Pinto, F. D. and Adamo, H. P. (2002). Deletions in the acidic lipid-binding region of the plasma membrane Ca2+ pump - A mutant with high affinity for Ca^{2+} resembling the acidic lipid-activated enzyme. *Journal of Biological Chemistry* **277**, 12784-12789.

Ritchie, M. F., Samakai, E. and Soboloff, J. (2012). STIM1 is required for attenuation of PMCA-mediated Ca2+ clearance during T-cell activation. *Embo Journal* **31**, 1123-1133.

Roy, A., Kucukural, A. and Zhang, Y. (2010). I-TASSER: a unified platform for automated protein structure and function prediction. *Nature Protocols* **5**, 725-738.

Schill, N. J. and Anderson, R. A. (2009). Out, in and back again: PtdIns(4,5)P-2 regulates cadherin trafficking in epithelial morphogenesis. *Biochemical Journal* **418**, 247-260.

Shi, J., Birnbaumer, L., Large, W. A. and Albert, A. P. (2013). Myristoylated alanine-rich C kinase substrate coordinates native TRPC1 channel activation by phosphatidylinositol 4,5-bisphosphate and protein kinase C in vascular smooth muscle. *FASEB Journal*. doi: 10.1096/fj.13-238022

Snitsarev, V. A. and Taylor, C. W. (1999). Overshooting cytosolic Ca2+ signals evoked by capacitative Ca2+ entry result from delayed stimulation of a plasma membrane Ca2+ pump. *Cell Calcium* **25**, 409-417.

Strehler, E. E., Caride, A. J., Filoteo, A. G., Xiong, Y., Penniston, J. T. and Enyedi, A. (2007). Plasma membrane Ca2+ ATPases as dynamic regulators of cellular calcium handling. *Annals of the New York Academy of Sciences* **1099**, 226-36.

Strehler, E. E. and Zacharias, D. A. (2001). Role of alternative splicing in generating isoform diversity among plasma membrane calcium pumps. *Physiological Reviews* **81**, 21-50.

Suh, B. C. and Hille, B. (2008). PIP(2) is a necessary cofactor for ion channel function: How and why? *Annual Review of Biophysics* **37**, 175-195.

Szentpetery, Z., Balla, A., Kim, Y. J., Lemmon, M. A. and Balla, T. (2009). Live cell imaging with protein domains capable of recognizing phosphatidylinositol 4,5-bisphosphate; a comparative study. *Bmc Cell Biology* **10**.

Toyoshima, C., Nakasako, M., Nomura, H. and Ogawa, H. (2000). Crystal structure of the calcium pump of sarcoplasmic reticulum at 2.6 angstrom resolution. *Nature* **405**, 647-655.

Toyoshima, C., Nomura, H. and Tsuda, T. (2004). Lumenal gating mechanism revealed in calcium pump crystal structures with phosphate analogues. *Nature* **432**, 361-368.

Toyoshima, C., Shinoda, T., Ogawa, H. and Cornelius, F. (2009). Structural Aspects of Cation Pumping by P-Type Atpases. *Journal of Physiological Sciences* **59**, 95-95.

Trebak, M., Lemonnier, L., DeHaven, W., Wedel, B., Bird, G. and Putney, J. W. (2009). Complex functions of phosphatidylinositol 4,5-bisphosphate in regulation of TRPC5 cation channels. *Pflugers Archiv-European Journal of Physiology* **457**, 757-769.

van den Bogaart, G., Meyenberg, K., Risselada, H. J., Amin, H., Willig, K. I., Hubrich, B. E., Dier, M., Hell, S. W., Grubmuller, H., Diederichsen, U. et al. (2011). Membrane protein sequestering by ionic protein-lipid interactions. *Nature* **479**, 552-555.

van der Wal, J., Habets, R., Varnai, P., Balla, T. and Jalink, K. (2001). Monitoring agonist-induced phospholipase C activation in live cells by fluorescence resonance energy transfer. *Journal of Biological Chemistry* **276**, 15337-15344.

Varnai, P. and Balla, T. (2008). Live cell imaging of phosphoinositides with expressed inositide binding protein domains. *Methods* **46**, 167-176.

Verma, A. K., Filoteo, A. G., Stanford, D. R., Wieben, E. D., Penniston, J. T., Strehler, E. E., Fischer, R., Heim, R., Vogel, G., Mathews, S. et al. (1988). Complete Primary Structure of a Human-Plasma Membrane Ca-2+ Pump. *Journal of Biological Chemistry* **263**, 14152-14159.

Whorton, M. R. and MacKinnon, R. (2011). Crystal Structure of the Mammalian GIRK2 K+ Channel and Gating Regulation by G Proteins, PIP2, and Sodium. *Cell* **147**, 199-208.

Yamoah, E. N., Lumpkin, E. A., Dumont, R. A., Smith, P. J. S., Hudspeth, A. J. and Gillespie, P. G. (1998). Plasma membrane Ca^{2+}-ATPase extrudes Ca2+ from hair cell stereocilia. *Journal of Neuroscience* **18**, 610-624.

Zhao, H. Y., Williams, D. E., Shin, J. B., Brugger, B. and Gillespie, P. G. (2012). Large Membrane Domains in Hair Bundles Specify Spatially Constricted Radixin Activation. *Journal of Neuroscience* **32**, 4600-4609.

Zhao, Q., Logothetis, D. E. and Seguela, P. (2007). Regulation of ATP-gated P2X receptors by phosphoinositides. *Pflugers Archiv-European Journal of Physiology* **455**, 181-185.

Zvaritch, E., James, P., Vorherr, T., Falchetto, R., Modyanov, N. and Carafoli, E. (1990). Mapping of Functional Domains in the Plasma-Membrane Ca-2+ Pump Using Trypsin Proteolysis. *Biochemistry* **29**, 8070-8076.

Legends to Figures

Figure 1. The presence of PMCA proteins prevents the translocation of the PIP_2 sensor during ionomycin treatments. The PIP_2 sensor, $PH_{PLC\delta1}$-RFP was expressed alone or together with GFP-PMCA2wb in sh-HeLa cells; or together with GFP-PMCA4b-LA in HeLa cells. *Panel A* shows the distribution of the PIP_2 sensor and the PMCA constructs after one day transfection in resting cells. Graphs display the $PH_{PLC\delta1}$-RFP (*red*) and PMCA (*green*) signal intensity profiles along the line of interest marked on the confocal images. *Panel B* shows the same cells 2 minutes after the addition of 10 μM ionomycin. Scale bars, 10 μm.

Figure 2. The effect of active and inactive PMCA constructs on the translocation of the PIP_2 sensor during ionomycin treatments. *A,* sh-HeLa (*top* images) or HeLa (*middle* images) cells were transfected with $PH_{PLC\delta1}$-RFP alone or together with GFP-tagged PMCA4b-LA (*bottom* immages), as in Figure 1. The cells were treated by the addition of 2 μM, 5 μM and 10 μM ionomycin at 0, 6 and 12 minutes, respectively. The fluorescence of the PIP_2 sensor is shown before treatments, and 5 minutes after the addition of 2, 5, and 10 μM ionomycin, respectively. The translocation of the PIP_2 sensor is reflected as an increase of the RFP fluorescence in the cytosol. Scale bars, 10 μm. *B,* The graphs show the changes of $PH_{PLC\delta1}$-RFP cytosolic fluorescence intensity during the treatments. Fluorescence intensity ratio (F_t/F_0) was plotted as a function of time. Arrows indicate times (0, 6 and 12 minutes) when 2 μM, 5 μM and 10 μM ionomycin were added. The *grey* curves (*left panel*) show changes of cytosolic $PH_{PLC\delta1}$-RFP intensity values in sh-HeLa cells expressing the sensor without PMCA (Supplementary movie S1). *These* cells were distinguished depending on their sensitivity to ionomycin. The *red* curve shows the fluorescence of the $PH_{PLC\delta1}$-RFP sensor in sh-HeLa cells expressing GFP-PMCA2wb. *The right panel* shows the intensity values of the $PH_{PLC\delta1}$-RFP sensor in HeLa cells expressing GFP-PMCA4b-LA (*blue;* Supplementary movie S2) and the dead GFP-PMCA4b-LA (dPMCA4b-LA) pump (*turquoise*). *C, Frequency of cells responding to a given concentration of ionomycin with complete translocation of $PH_{PLC\delta1}$-RFP*. The frequency of cells not responding to inomycin is not shown. 3 independent experiments were performed (n=30-60 cells were counted). Statistical significance of differences between cells expressing or not the different PMCA construct was analyzed using $\chi 2$ test (***, $p<0.0001$; *, $p<0.05$)

Figure 3. Ca^{2+} transients in HeLa cells expressing active and inactive PMCA constructs treated with increasing concentrations of ionomycin. *A,* sh-HeLa and HeLa cells were transfected with the Ca^{2+} sensor, GCaMP2 alone or together with mCherry-tagged PMCA constructs. The cells were treated with 2 μM, 5 μM and then 10 μM ionomycin the same way as in the experiment shown in Figure 2. The fluorescence of the GCaMP2 sensor is shown before the treatment and after the addition of 10 μM ionomycin. Scale bars, 10 μm. *B,* The graphs show the changes of the cytosolic fluorescence

intensity of the GCaMP2 sensor, during the treatments. Fluorescence intensity ratio (F_t/F_0) was plotted as a function of time. Arrows indicate times when 2 μM, 5 μM and 10 μM ionomycin were added. The *black* curve (*left panel*) shows the changes in the GCaMP2 intensity values in sh-HeLa cells expressing the GCaMP2 sensor without PMCA. The *red* curve shows the fluorescence of the GCaMP2 sensor in sh-HeLa cells expressing mCherry-PMCA2wb. *The right panel* shows the intensity values of GCaMP2 in HeLa cells expressing mCherry-PMCA4b-LA (*blue*) and the dead mCherry-PMCA4b-LA (dPMCA4b-LA) pump (*turquoise*). Values represent mean ± S.E. of 15-30 cells from 2-3 independent experiments.

Figure 4. Effect of PMCA constructs on PIP_2 and Ca^{2+} signaling during receptor-mediated PLC activation. sh-HeLa cells were transfected with $PH_{PLC\delta1}$-RFP or the GCaMP2 sensor alone or together with GFP- or mCherry-tagged PMCA2wb. HeLa cells were co-transfected with either $PH_{PLC\delta1}$-RFP or GCaMP2 and the appropriate PMCA4b-LA or dead PMCA4b-LA constructs. $PH_{PLC\delta1}$-RFP and the GFP-tagged PMCA constructs were used *in panels A1 and B1*, GCaMP2 and the mCherry-tagged PMCA constructs *in panels A2 and B2*, as indicated. Cells were stimulated with 100 μM ATP and 100 μM histamine (2 minutes after ATP) in the absence of Ca^{2+}. The extracellular media was replenished by 2 mM Ca^{2+} after 5 minutes. More details of the experimental protocol are described in Figure S2. *Panel A1 and B1* show the $PH_{PLC\delta1}$-RFP signals, *Panel A2 and B2* show the Ca^{2+} transients measured in cells expressing the sensor alone (*black*), together with GFP-PMCA4b-LA (*blue*), GFP-dPMCA4b-LA (*turquoise*) or GFP-PMCA2wb (*red*), as indicated. Values represent mean ± S.E. of 10-30 cells from 2-3 independent experiments. *C1 and C2*, Areas of Ca^{2+} (GCaMP2) signals under the ATP peaks (*C1*) and Ca^{2+} entry peaks (*C2*) (arbitrary units). Data are means ± S.E. of 15-60 cells analyzed from 3 independent experiments. Asterisks represent significant difference between bars indicated with brackets (** $p<0.01$, *** $p<0.0001$, Student's t-test).

Figure 5. The blue collar is present in PMCA but lacking in SERCA. *A,* Ribbon diagram of the model of PMCA4b, made as described in Methods. Arginines and Lysines in the lower half of the stalk, near the cytoplasmic surface of the membrane comprise the blue collar; they are shown in space-filling blue. The *B molecule* shows the electrostatic potential at the surface of the same model, with red representing negatively charged surface, white neutral and blue positive. The *C molecule* is the same as the second one, except that the inserts which are not homologous to SERCA were omitted. As that part of the figure shows, those inserts contributed mainly to the negatively charged surface regions; their omission did not affect the blue collar. *D,* The E1 conformation of SERCA (1T5S) which was used to make the PMCA model. This structure lacks the blue collar.

Figure 6. Four pockets which bind PIP_2. *Panel A* shows PMCA4b with the 4 pockets embedded in the bilayer. On the left, for comparison, is the surface potential of PMCA4b. Pocket R993 is outlined

by a rectangle, and the area of the rectangle is shown in a stick model *in panel C. In panel B* a slice through the model shows the pockets from above. The residues of pocket R993 are highlighted in green, pocket R914 in blue, pocket K980 in purple and pocket K173 in red The relative energies of the PIP_2-pocket complexes are shown *in panel D,* in which 3SPI is the energy of the complex in a known PIP_2 binding protein. *Panel E* shows which residues are involved in each pocket.

Figure 1

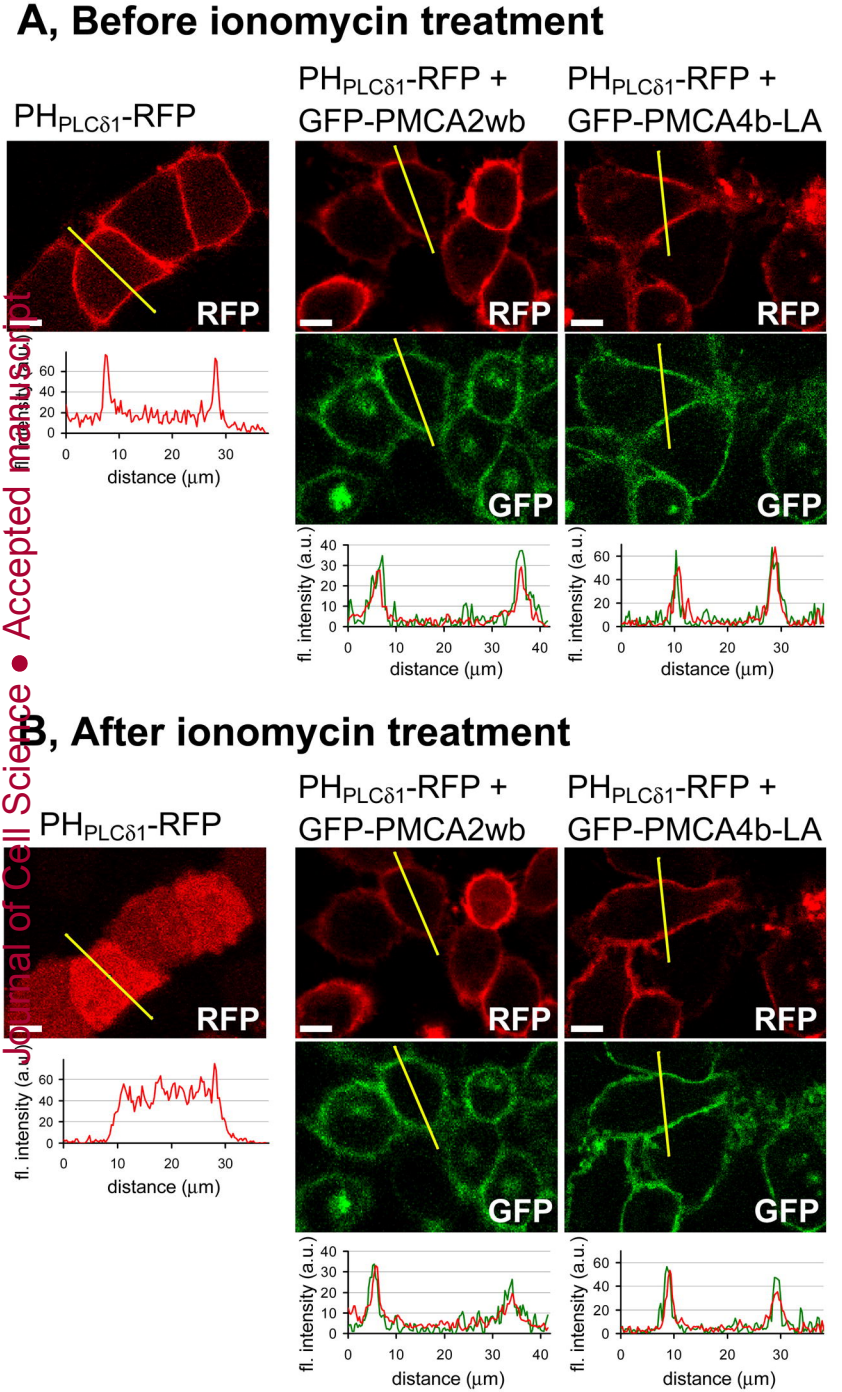

Figure 2

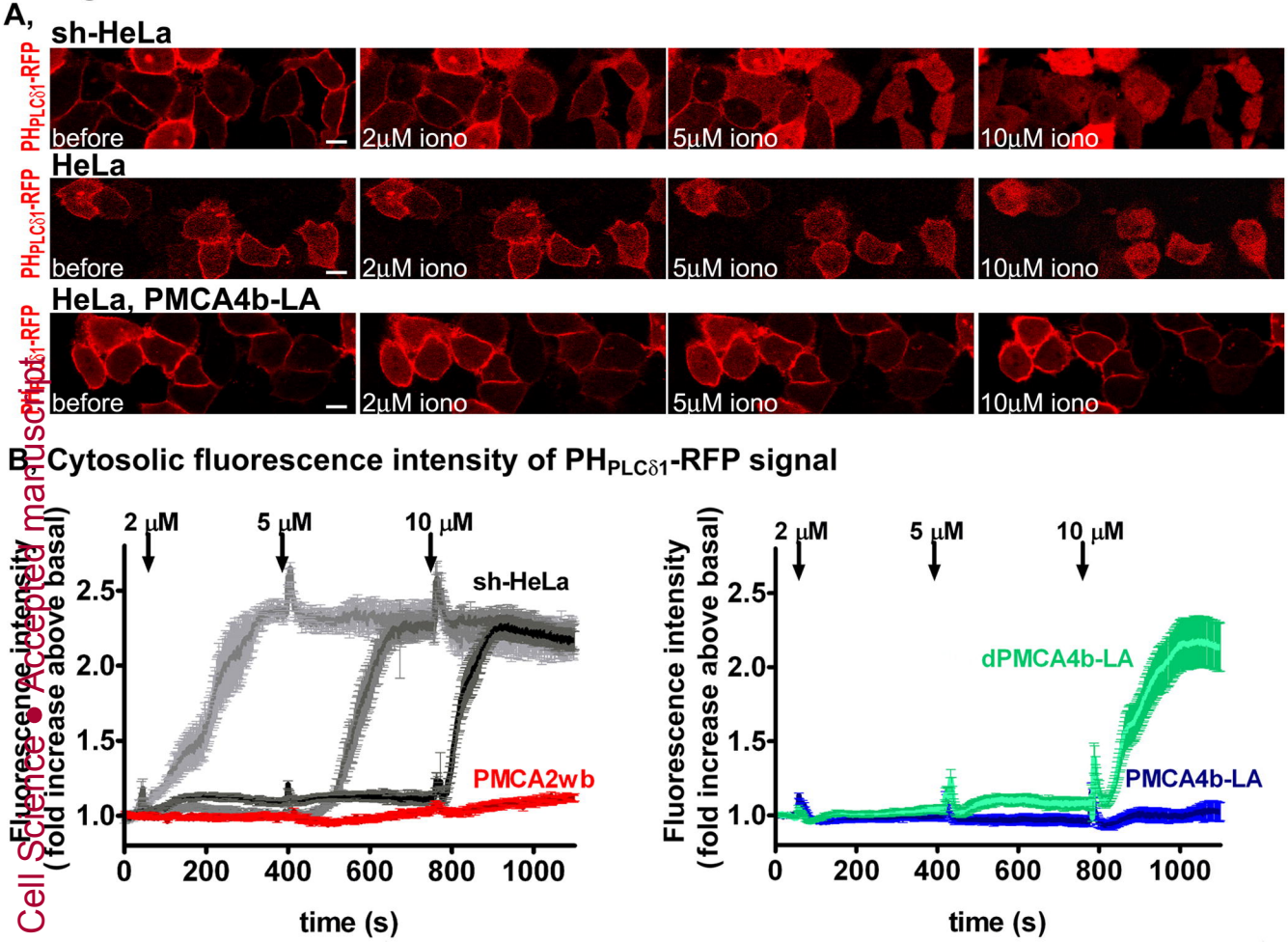

Figure 3

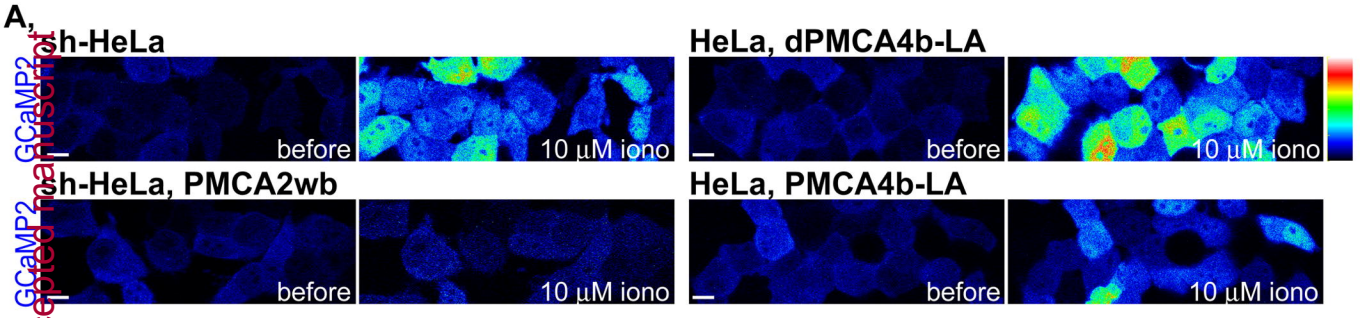

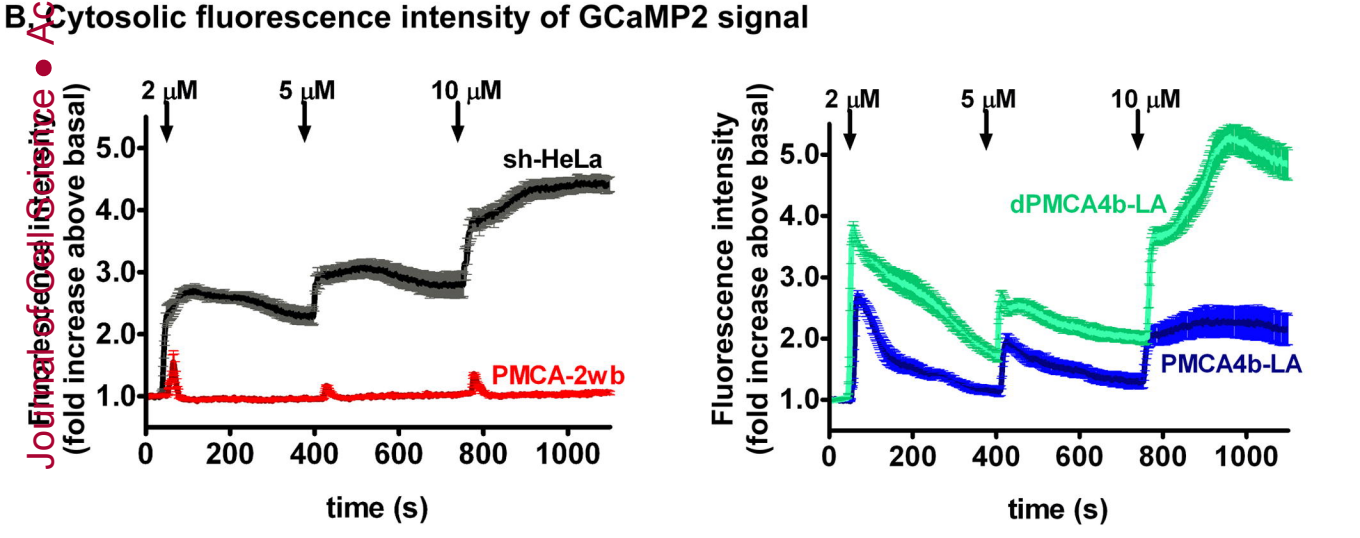

Figure 4

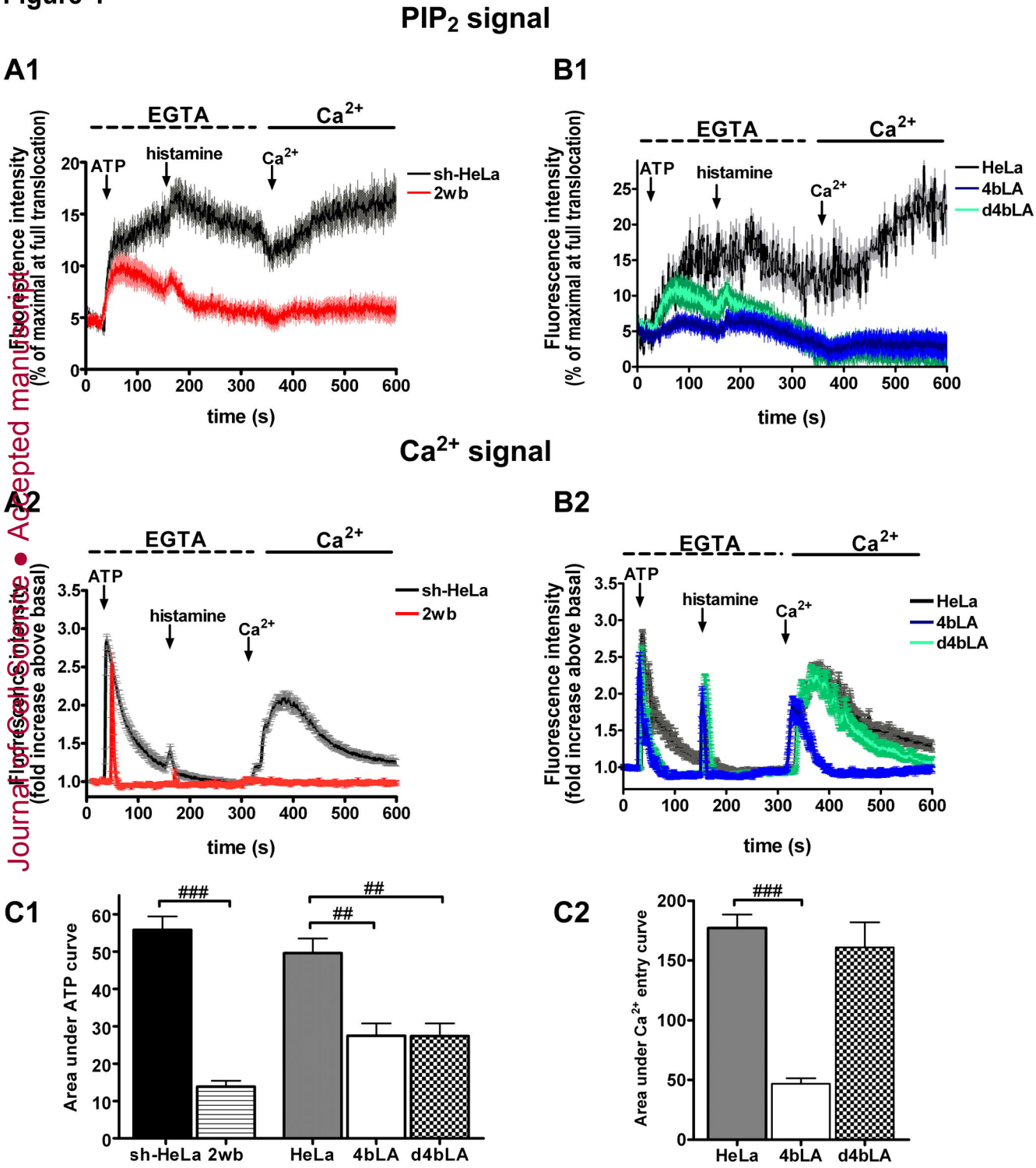

Figure 5

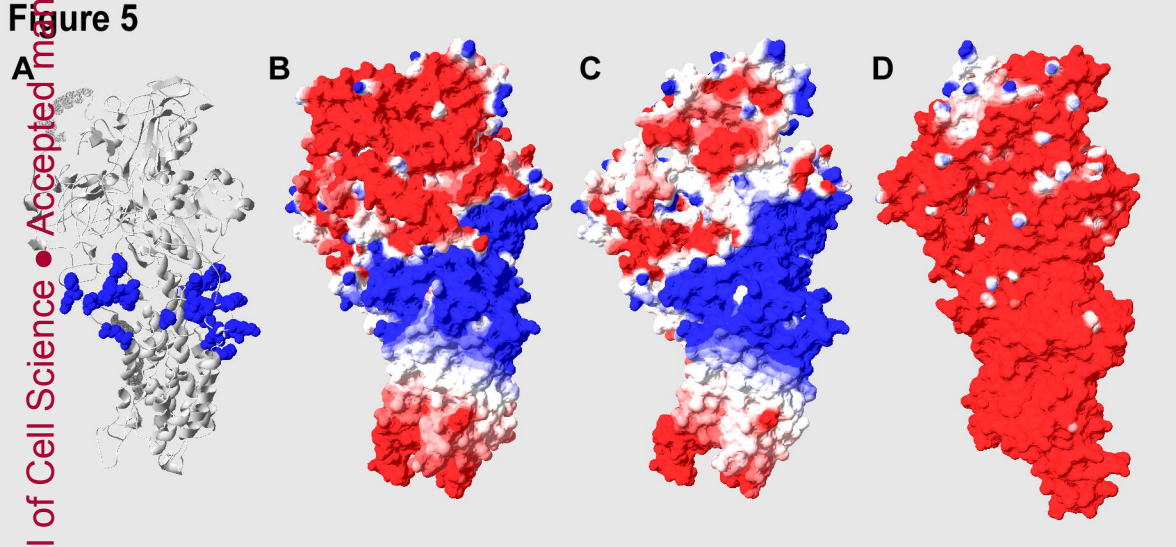

Figure 6

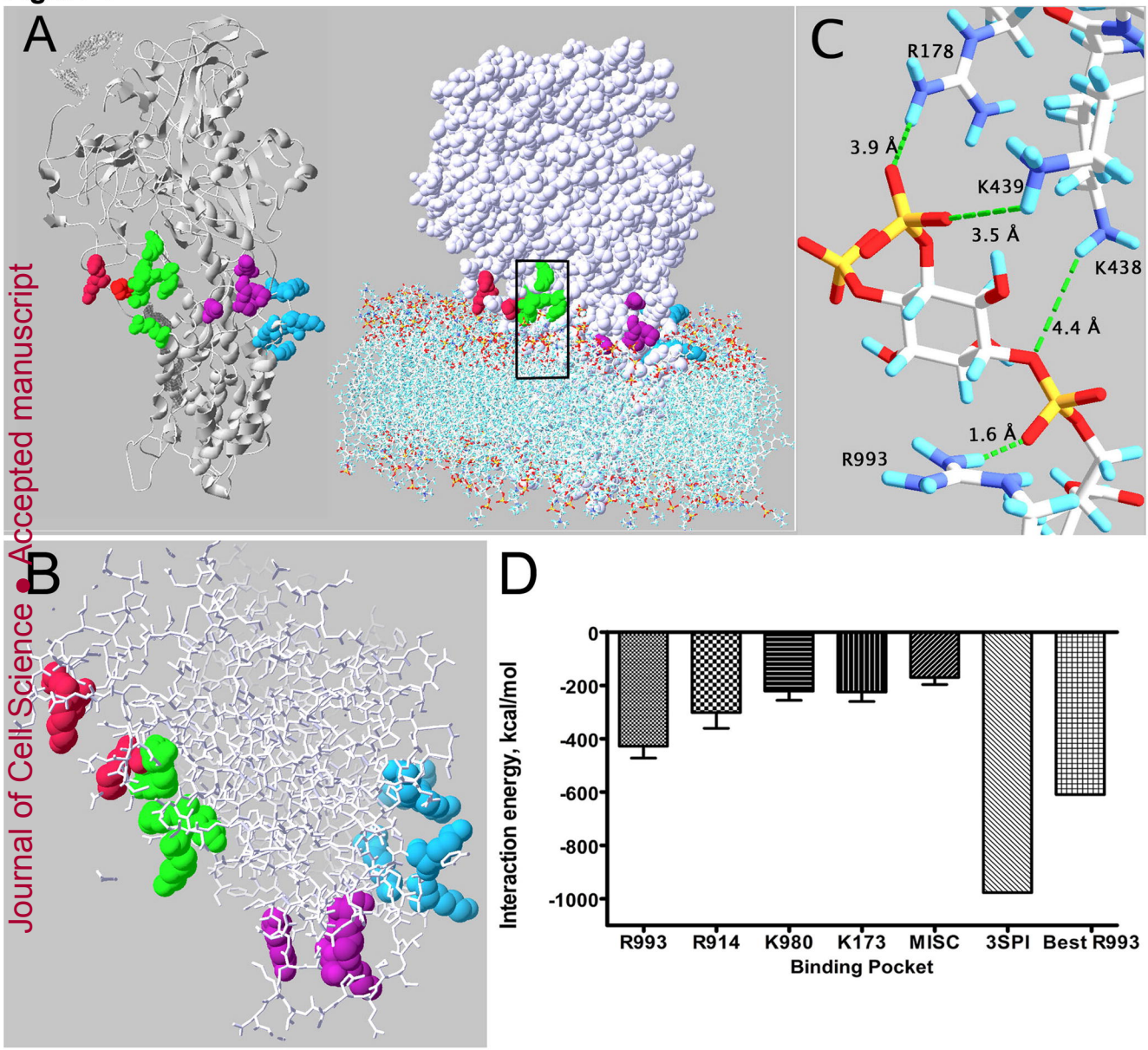

E

Pocket R993	Pocket R914	Pocket K980	Pocket K173
E174, R178, K438, K439, K442, R993	*K909, R914, K918 R1052, K1055, K1058*	*K901, R979, K980 H982, K985, K1055*	*K88, K89, K173 R178*

Table 1.

The frequency with which each lipid binds to multiple amino acids.

	total	singles	doubles	triples	quads	Eav, kcal/mol
PC	1013	88,3%	11,1%	0,7%	0,0%	-39,2
PE	1297	88,9%	10,1%	1,0%	0,0%	-38,1
PS	718	97,4%	2,6%	0,0%	0,0%	-57,6
PI	743	98,0%	2,0%	0,0%	0,0%	-71,1
PIP_2	2347	51,7%	25,5%	15,7%	7,1%	-245,4

PC and PE bind to 2 (doubles) or 3 (triples) amino acids about 12% of the total interactions

PI and PS bind to multiple residues at an even lower frequency, about 2%

PIP_2 binds to multiple residues much more frequently (48.3%), with many triples and quads. Eav is the average energy of binding per lipid. In the case of multiple binding, all the interactions are included. Eav is much higher for PIP_2 because of the multiple bindings, many of which are quite strong.

To compile Table 1, all of the saved coordinates from the 15 molecular dynamics runs were analyzed. The coordinates were saved every 0.2 nsec, except that the first few runs were saved more frequently.